SCIENCE CHINA
Information Sciences

• RESEARCH PAPER •

October 2025, Vol. 68, Iss. 10, 202301:1–202301:17
https://doi.org/10.1007/s11432-025-4525-7

Relay selection and optimal deployment for mmWave-FD UAV-assisted 6G communication systems over N-Rayleigh channels

Luoyu GAO, Siye WANG*, Yanzhao HOU, Wenbo XU & Kai NIU

School of Artificial Intelligence, Beijing University of Posts and Telecommunications, Beijing 100876, China

Received 14 January 2025/Revised 13 June 2025/Accepted 23 July 2025/Published online 11 August 2025

Abstract The rapid evolution of the 6G communication landscape demands innovative approaches to address its increasing complexity. Integrated sensing and communication (ISAC) emerges as a pivotal strategy, exploiting the synergy between sensing and communication to enhance the capabilities of the 6G network. This paper examines the deployment of unmanned aerial vehicles (UAVs) as dynamic relays in full-duplex millimeter-wave (mmWave) environments, a key direction for ISAC within 6G frameworks. We focus on urban communication scenarios, specifically the base station-multi-UAV-mobile ground user (BMUM) and mobile ground user-multi-UAV-mobile ground user (MMUM) configurations, where UAVs are employed to mitigate the challenges of air-to-ground and mmWave large-scale fading. Through rigorous mathematical modeling, we present analytical solutions for the outage probability across various UAV relay selection strategies in N-Rayleigh channel conditions, validated by Monte Carlo simulations. The findings not only enhance the reliability and performance of 6G networks but also advance our understanding of the critical role ISAC plays in optimizing future communication technologies.

Keywords relay selection, full duplex, mmWave, UAV, N-Rayleigh

Citation Gao L Y, Wang S Y, Hou Y Z, et al. Relay selection and optimal deployment for mmWave-FD UAV-assisted 6G communication systems over N-Rayleigh channels. Sci China Inf Sci, 2025, 68(10): 202301, https://doi.org/10.1007/s11432-025-4525-7

1 Introduction

The rapid expansion of services in areas such as smart homes, industrial automation, smart cities, precision agriculture, and vehicular networks underscores the escalating complexity and diversity of communication requirements. These evolving demands are driving the development of 6G communication architectures designed to support extensive, low-latency, highly reliable data exchanges crucial for urban management, and to provide networks capable of extensive coverage with low power consumption suitable for agriculture [1, 2]. Traditional communication frameworks, often constrained by fixed infrastructures, struggle to meet these advanced requirements. 6G networks, with their inherent flexibility and advanced capabilities, are poised to overcome the limitations of previous generations by offering enhanced efficiency, flexibility, and drastically reduced latency, making them well-suited for dynamic environments or scenarios with limited infrastructure.

In this emerging context, the deep integration of communication and sensing has become a pivotal strategy, giving rise to integrated sensing and communication (ISAC). Operating at ultra-high frequencies from 30 to 300 GHz, millimeter wave (mmWave) technology is at the forefront of this transition. It provides extremely high data transmission rates and large bandwidths, ideal for managing the massive data transmission requirements of modern applications. The high-frequency characteristics of mmWave not only facilitate high-speed data communication but also enable high-precision environmental sensing, such as vehicle positioning and tracking in advanced transportation systems. This capability is essential for the effective implementation of ISAC strategies, leveraging the strengths of 6G technologies to enhance both communication reliability and environmental interaction across various settings [3].

The advancement of unmanned aerial vehicle (UAV) technology injects new vitality into ISAC. UAVs, known for their low cost, high flexibility, and mobility, are extensively utilized across various fields,

* Corresponding author (email: wsy@bupt.edu.cn)

including surveillance, search and rescue, and disaster response. In ISAC scenarios, UAVs excel as mobile platforms. On one hand, they serve as relay nodes, overcoming the coverage limitations of mmWave by flexibly establishing line-of-sight (LoS) communication links, significantly expanding the communication range, and enhancing communication service quality [4]. On the other hand, UAVs, equipped with various sensors and combined with the sensing capabilities of mmWave technology, rapidly and comprehensively survey large areas. For instance, in complex terrains or areas with severe signal obstructions, UAVs swiftly adjust their positions to gather more comprehensive environmental information, thus ensuring stable and smooth communication.

The organic combination of UAVs and mmWave demonstrates tremendous potential in the field of ISAC. On one hand, UAVs can overcome the range limitations of mmWave. As mentioned earlier, mmWave is susceptible to high path loss and blockages, restricting its communication range when deployed on the ground or in fixed positions. With their ability to flexibly adjust positions and establish line-of-sight links, UAVs can serve as mobile relay platforms for mmWave signals. Strategically deployed, they can extend the reach of mmWave communication, utilizing their high data rates and large bandwidths over a wider area, crucial for meeting the extensive coverage demands of IoT applications. On the other hand, mmWave enhances the performance of UAV-assisted relay systems. The high data rates and large bandwidths of mmWave significantly boost the transmission efficiency of data relayed by UAVs. In scenarios with a large volume of data transmission, such as smart city traffic monitoring or industrial automation, the combination of UAVs and mmWave ensures quick and reliable data transmission. Additionally, the highly directional nature of mmWave antennas reduces interference in the communication links established by UAVs, further improving communication quality and enabling a more stable and efficient IoT system.

Motivated by these considerations, UAV-assisted relay communication has become a critical enabler for IoT scenarios, addressing the limitations of conventional ground-based relays in coverage and mobility. Furthermore, UAVs offer flexible scheduling capabilities that optimize resource allocation, thereby enhancing the overall performance of IoT communication systems.

1.1 Related work

In the field of UAV-assisted relay communication systems, numerous scholars have proposed various optimization strategies to enhance system efficiency, security, and energy management. In terms of trajectory and transmission power optimization, Li et al. [5] studied the optimal flight altitude of UAVs in relay networks to improve signal coverage and network performance. Liu et al. [6] developed an algorithm that significantly enhances the communication quality of multi-link relay systems by precisely adjusting the flight paths and power settings of UAVs. This optimization not only improves the reliability of data transmission but also reduces energy consumption, providing a new direction for the design of multi-hop UAV networks [7, 8].

In the area of network efficiency and management for multiple UAV systems, numerous researchers have proposed innovative strategies and technologies to address the complex challenges in dynamic network environments. Ding et al. and Pan et al. [9, 10] enhanced the communication efficiency and stability of dynamic multi-hop UAV networks by exploring packet routing and resource allocation strategies. Additionally, Pan et al. and Sharma et al. [11, 12] further optimized the network's configuration and operation by studying the network layout and communication strategies of multi-UAV relay systems.

Regarding the coordination and management of multiple UAV systems, Ernest et al. [13] highlighted the application potential of hybrid duplex communication technologies in enhancing communication efficiency and network flexibility. Yanmaz [14] focused on dynamic relay selection and positioning issues within cooperative UAV networks, proposing methods to enhance network performance and communication stability. Meanwhile, Zhang et al. and Yin et al. [15, 16] proposed a cooperative UAV communication system and air-to-ground relay communication planning in their research, greatly improving the overall performance and responsiveness of the network.

In terms of security and confidentiality, a series of studies have been dedicated to enhancing the security defenses of UAV communication systems through innovative strategies. Hu et al. [17] enhanced the security barrier of the network by introducing a proactive eavesdropping strategy, which preemptively intercepts potential threat sources. At the same time, the research by Lee and Wang et al. [18,19] focused on optimizing relay selection and communication protocols, effectively enhancing communication secrecy and reducing potential security threats. Additionally, Bao et al. [2] analyzed the secrecy outage perfor-

mance in UAV-assisted communication systems, assessing security performance in various operational scenarios to provide crucial security metrics for the system's practical deployment. Kong et al. [20] proposed a strategy to balance security and reliability in UAV-assisted communication systems, considering maintaining communication continuity and reliability while enhancing security. Wang et al. [21] demonstrated how to simultaneously maximize secrecy and energy efficiency in UAV-supported communication networks, proposing a comprehensive strategy for security and energy optimization that maintains high secrecy while optimizing energy use.

In energy efficiency and power management, the studies by He et al. and Ji et al. [22, 23] respectively focused on UAV-supported communication systems and fixed-wing UAV networks. By optimizing flight strategies and energy settings, their research significantly reduced energy consumption and extended the operational time of UAVs. These achievements highlight the importance of effectively managing energy consumption in designing UAV relay systems to ensure continuous operation and efficiency. Additionally, Woo et al. [24] proposed a virtual full-duplex relay scheme and its adjustment algorithm, aimed at enhancing the spectral efficiency of UAV networks, thereby optimizing the use of communication resources. Sun et al. [25] focused on how to enhance UAV energy efficiency while ensuring communication security. By developing optimized algorithms, not only did he reduce energy consumption, but he also enhanced the system security. Huang et al. [26] explored methods and efficiencies of real-time data collection in UAV-assisted wireless networks. This research, through improvements in data collection technology, optimized the timeliness and accuracy of data, further enhancing the network operational efficiency.

Innovation in UAV communication technology is a key driver for advancing the field. Zhang et al. [27] investigated a resource allocation problem for a multi-UAV assisted ISAC system. Ref. [28] addressed how the uncertain locations of ground users impact UAV trajectory design in UAV-assisted integrated communication and sensing networks. In another study [29], authors explore the content delivery and target sensing problems in UAV-enabled ISAC networks. Liu et al. [30] examined an ISAC-UAV assisted secure communication system amidst multiple eavesdroppers. To tackle the signaling overhead inherent in traditional ISAC, Duan et al. [31] proposed a deep learning-based end-to-end predictive beamforming method, which leverages an encoder-decoder network to extract spatiotemporal features from historical channels, thereby enhancing sensing accuracy while maintaining communication performance. Advanced beamforming remains a focal point of research. Cui et al. [32] presented a novel dual identity association (DIA)-based ISAC approach, which is the first solution that enables specific, fast, and accurate beamforming towards multiple UAVs. Similarly, leveraging artificial intelligence for beamforming prediction, Wu et al. [33] developed a multi-reward double deep Q-network for UAV-reconfigurable intelligent surface (RIS) assisted THz systems, enabling efficient end-to-end beam selection that jointly optimizes the communication rate and power consumption. Furthermore, researchers are exploring the intersection of advanced multiple access schemes with deployment and security. Wang et al. [34] explored joint terminal-UAV association issues, aimed at optimizing network coverage and service quality. Su et al. [35] explored optimal deployment strategies for UAVs in providing network coverage, aimed at achieving the broadest geographical coverage. Wang et al. [36] investigated secure beamforming and deployment optimization in rate-splitting multiple access-based UAV networks, proposing a joint optimization framework that significantly outperforms conventional space division multiple access (SDMA) and non-orthogonal multiple access (NOMA) in maximizing the sum secrecy rate. In [37], the joint optimization problem of relay selection and transmission scheduling is studied in the UAV-assisted two-way relay system of millimeter-wave communication. These innovations not only demonstrate the application of UAV technology in improving network efficiency and functionality but also highlight its importance in secure, reliable, and efficient communication.

1.2 Summary of contributions

This paper investigates relay selection strategies in UAV-assisted multi-relay communication systems, considering both UAV air-to-ground (A2G) path fading and mmWave large-scale fading effects. By deriving mathematical expressions for outage probability and conducting comprehensive performance analyses under various relay selection strategies, this study provides key insights into improving communication reliability and efficiency in ISAC systems. The main contributions of this paper are as follows.

• Proposes two full-duplex (FD) mobile communication scenarios using drones as relays: (a) a base station-multi-drone-mobile ground user (BMUM) scenario, wherein the communication between the base station (BS) and the mobile ground user (MGU) is modeled using a hybrid Rayleigh channel; (b) a mobile

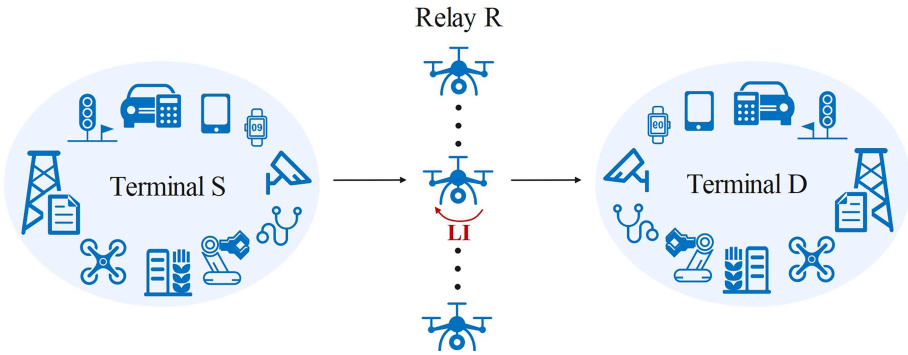

Figure 1 (Color online) Multi-relay communication system model.

ground user-multi-UAV-mobile ground user (MMUM) scenario, wherein communication between the UAV and MGU is modeled using an N-Rayleigh fading channel. In both scenarios, UAV A2G path fading and mmWave large-scale fading are considered, which elucidate the characteristics of UAV millimeter-wave communication and reflect actual communication conditions.

• In the BMUM and MMUM scenarios, we study the impact of four relay selection strategies on the communication system's reliability. Considering the impacts of UAV path fading and millimeter wave large-scale fading, we deduce the analytical solution for the outage probability under each strategy through mathematical analysis, and verify its accuracy.

The aforementioned communication scenarios have been carefully selected based on their distinct operational significance and practical relevance for future 6G deployments. Specifically, the BMUM scenario is highly applicable to densely populated urban environments, where fixed base stations depend on UAV-assisted relays to mitigate line-of-sight blockages and ensure reliable coverage for mobile users. Conversely, the MMUM scenario addresses the communication requirements of rapidly evolving and decentralized contexts, such as emergency responses, disaster recovery operations, or temporary event setups lacking established infrastructure. Clearly delineating these scenarios underscores the necessity for customized relay selection strategies, thereby optimizing UAV deployment across diverse communication contexts in ISAC-driven 6G networks.

The remainder of the paper is organized as follows. Section 2 introduces the proposed communication scenarios, system model, and channel characteristics, including UAV path fading. Section 3 explores four relay selection strategies and deduces the corresponding outage probability expressions. Section 4 presents simulation results to validate the theoretical findings. Finally, Section 5 concludes the paper and outlines future research directions.

2 System model

Figure 1 illustrates a model of a multi-relay communication system composed of a source node s, N UAV relays r, and a destination node d. The source node s and the destination node d communicate in half-duplex (HD), whereas the UAV relays r communicate in FD mode. Due to the non-negligible occlusion caused by the buildings, direct communication between the source node s and the destination node d is difficult. Each time slot will have a single relay selected and participating in the information transfer. Due to the FD communication mode of the selected relay, it will receive and transmit data concurrently, making loop interference inevitable.

Assuming that at time slot t, relay node r_i is selected for communication between the source and destination nodes via the relay selection strategy. Therefore, the multi-relay communication system can be simplified to a single-relay communication system, as illustrated in Figure 2, where h denotes the flying altitude of the UAV relay r_i, and d_{sr_i} and d_{r_id} respectively signify the horizontal distances between the source node s and the destination node d and between the destination node d and the relay r_i.

In this study, the large-scale path loss models incorporated account for the unique characteristics of A2G communication and mmWave frequencies. Specifically, in dense urban environments with numerous buildings, the wireless signal transmission experiences additional losses. These are modeled taking into consideration both the direct LoS and multiple non-line-of-sight (NLoS) components that are prevalent in UAV communication scenarios. For mmWave frequencies, the model further incorporates the atmospheric

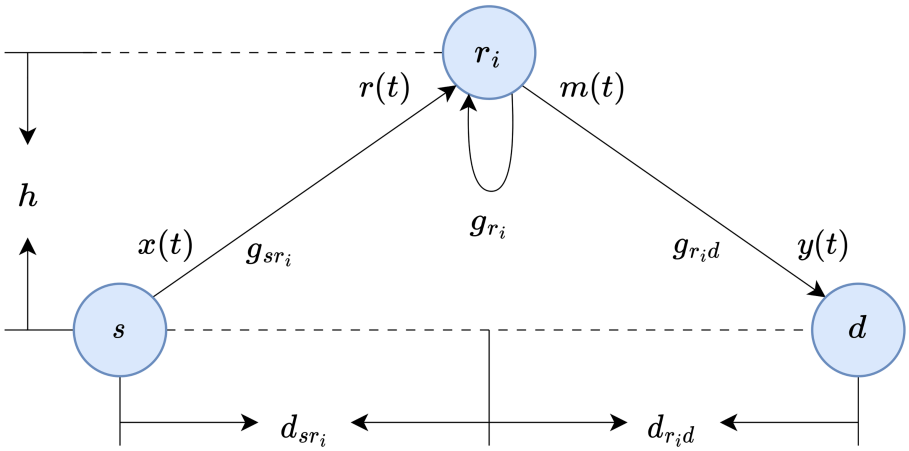

Figure 2 (Color online) Simplified system model.

and rain attenuation which are significant at higher frequencies. Therefore, the path loss between the source node s and the destination node d and between the destination node d the relay r_i, can be respectively written as

$$\begin{aligned}\Omega_{sr_i}&=\frac{\eta_{\mathrm{LoS}}-\eta_{\mathrm{NLoS}}}{1+\alpha\mathrm{e}^{\left(-\beta\left[\frac{180}{\pi}\arctan\left(\frac{h}{d_{sr_i}}\right)-\alpha\right]\right)}}+20\log_{10}\left(\frac{4\pi f_{mm}}{\mathrm{c}}\sqrt{h^2+d_{sr_i}^2}\right)+\eta_{\mathrm{NLoS}}+(\alpha_{\mathrm{atm}}+\alpha_{\mathrm{rain}})\sqrt{h^2+d_{sr_i}^2},\\ \Omega_{r_id}&=\frac{\eta_{\mathrm{LoS}}-\eta_{\mathrm{NLoS}}}{1+\alpha\mathrm{e}^{\left(-\beta\left[\frac{180}{\pi}\arctan\left(\frac{h}{d_{r_id}}\right)-\alpha\right]\right)}}+20\log_{10}\left(\frac{4\pi f_{mm}}{\mathrm{c}}\sqrt{h^2+d_{r_id}^2}\right)+\eta_{\mathrm{NLoS}}+(\alpha_{\mathrm{atm}}+\alpha_{\mathrm{rain}})\sqrt{h^2+d_{r_id}^2},\end{aligned} \tag{1}$$

where $\alpha,\beta,\eta_{\mathrm{LoS}}$ and η_{NLOS} are the constants associated with the propagation environment in the communication link, and h is the flight altitude of the UAV relay, f is the carrier frequency, c is the speed of light, α_{atm} represents the attenuation coefficient caused by atmospheric absorption, α_{rain} represents the attenuation coefficient caused by rain. Then the absolute path loss of link s-r_i and link r_i-d can be obtained from (1) as

$$\begin{aligned}Q_{sr_i}&=10^{\frac{\Omega_{sr_i}}{10}},\\ Q_{r_id}&=10^{\frac{\Omega_{r_id}}{10}}.\end{aligned} \tag{2}$$

Due to the inherent loop interference problem introduced by full-duplex relaying, in addition to the conventional links s-r_i and r_i-d, link r_i-r_i also exists, denoted by g_{sr_i}, g_{r_id}, and g_{r_i} for their respective instantaneous channel parameters. The full-duplex decode-and-forward (DF) relay r_i then receives the signal $r(t)$ from the source node s and performs decoding and recoding processing, before sending the processed signal $m(t)$ to the destination node d. The received signal $r(t)$ can be expressed in the following way:

$$r(t)=\sqrt{\frac{P_s}{Q_{sr_i}}}g_{sr_i}x(t)+\sqrt{\frac{P_{r_i}}{Q_{r_id}}}g_{r_i}m(t)+n_{r_i}, \tag{3}$$

where P_s and P_{r_i} denote the transmit power of the source node s and the DF relay r_i, and n_{r_i} denotes the noise at the DF forwarding relay r_i, which can be modeled as additive Complex Gaussian white noise with a mean of zero and a variance of N_r. The second term in this expression denotes the loop interference introduced by the full-duplex communication method.

The signal $y(t)$ received by the destination node via relay r_i can then be expressed as

$$y(t)=\sqrt{\frac{P_{r_i}}{Q_{r_id}}}g_{r_id}m(t)+n_d, \tag{4}$$

where n_d denotes the additive complex Gaussian white noise at the destination node d with zero mean and variance N_d.

According to previous analysis, the path loss between source node s and DF forwarding relay r_i, as well as the path loss between relay r_i and destination node d, is not negligible due to obstructions such as buildings. The signal-to-noise ratios of the s-r_i and r_i-d links can then be expressed as

$$\overline{\gamma}_{sr_i} = \frac{P_s \left|g_{sr_i}\right|^2}{Q_{sr_i} N_r}, \tag{5}$$

$$\gamma_{r_i} = \frac{P_r \left|g_{r_i}\right|^2}{N_r}, \tag{6}$$

$$\gamma_{sr_i} = \frac{\overline{\gamma}_{sr_i}}{1+\gamma_{r_i}}, \tag{7}$$

$$\gamma_{r_i d} = \frac{P_r \left|g_{r_i d}\right|^2}{Q_{r_i d} N_d}. \tag{8}$$

Therefore, the instantaneous channel capacity of this full-duplex DF multi-relay communication system can be calculated as

$$C_i^{\mathrm{FD}} = \log_2\left(1+\min\left\{\gamma_{sr_i}, \gamma_{r_i d}\right\}\right). \tag{9}$$

In densely populated urban areas, the propagation environment for UAV-assisted communications is highly complex, characterized by multipath propagation, severe shadowing, and rich scattering caused by numerous obstacles and reflectors distributed at various altitudes. Traditional single-Rayleigh or Nakagami-m models are often inadequate for accurately capturing these compounded fading effects. To address this, we employ the N-Rayleigh channel model, which is widely recognized as a small-scale fading channel model whose probability distribution closely matches the observed amplitude fading in a broad range of wireless environments. By considering the cascade of multiple independent Rayleigh processes, the N-Rayleigh model offers a more realistic and flexible representation of the compounded fading experienced in UAV-to-ground communications, particularly in NLoS urban environments. Based on these considerations, we formulate two distinct multi-relay mobile communication scenarios—BMUM and MMUM—as described in Section 1. Both scenarios employ the N-Rayleigh fading model to accurately reflect the complex and practical channel conditions encountered in UAV-assisted 6G networks.

• BMUM scenario

The BMUM scenario illustrates the information transmission process between the base station and the mobile ground user. The channels g_{sr_i} and g_{r_i} are modeled as Rayleigh fading channels in this scenario, while the channel $g_{r_i d}$ is modeled as N-Rayleigh fading channel. According to the expressions of signal-to-noise ratio (SNR) (5)–(8), the expressions for the probability density functions (PDFs) of the SNRs are obtained as follows:

$$f_{\overline{\gamma}_{sr_i}}(x) = b_{sr_i} \mathrm{e}^{-b_{sr_i} x}, \tag{10}$$

$$\begin{aligned} f_{\gamma_{r_i d}}(x) &= \frac{a_{r_i d}^m x^{c-1}}{n\Gamma(m)} \mathrm{e}^{-a_{r_i d}^m x^{\frac{1}{n}}} \\ &\approx \frac{a_{r_i d}^m}{n\Gamma(m)} \sum_{k=1}^{\infty} \frac{(-a_{r_i d}^m)^k}{k!} x^{c-1+\frac{k}{n}}, \end{aligned} \tag{11}$$

$$f_{\gamma_{r_i}}(x) = b_r \mathrm{e}^{-b_r x}, \tag{12}$$

where $m = 0.6102n + 0.4263, \Omega = 0.8808n^{-0.9661} + 1.12, c = m/n$, $\Gamma(m)$ represents the Gamma function with parameter m, $a_{r_i d} = \frac{2m}{\Omega}(\frac{Q_{r_i d} N_d}{P_r \sigma_{r_i d}^2})^{\frac{1}{n}}, b_{sr_i} = \frac{N_r Q_{sr_i}}{P_s \sigma_{sr_i}^2}, b_r = \frac{N_r}{P_r \sigma_r^2}, \sigma_{sr_i}^2, \sigma_{r_i d}^2$ and σ_r^2 are the variance of $g_{sr_i}, g_{r_i d}$ and g_{r_i}. Therefore, the cumulative distribution functions (CDFs) of $\overline{\gamma}_{sr_i}, \gamma_{r_i d}$ and γ_{r_i} are

$$F_{\overline{\gamma}_{sr_i}}(x) = 1 - \mathrm{e}^{-b_{sr_i} x}, \tag{13}$$

$$F_{\gamma_{r_i d}}(x) \approx \frac{a_{r_i d}^m}{n\Gamma(m)} \sum_{k=1}^{\infty} \frac{(-a_{r_i d})^k x^{c+\frac{k}{n}}}{k!\left(c+\frac{k}{n}\right)}, \tag{14}$$

$$F_{\gamma_{r_i}}(x) = 1 - \mathrm{e}^{-b_{r_i} x}. \tag{15}$$

According to (7), (12), and (13), the CDF of γ_{sr_i} can be written as

$$F_{\gamma_{sr_i}}(x) = \Pr\left[\frac{\overline{\gamma}_{sr_i}}{1+\gamma_{r_i}} < x\right] = 1 - \frac{b_r \mathrm{e}^{-b_{sr_i}x}}{b_r + b_{sr_i}x}. \tag{16}$$

• MMUM scenario

The MMUM scenario describes communication between two mobile ground users. Based on the communication characteristics in this scenario, g_{r_i} is modeled as a Rayleigh fading channel, whereas g_{sr_i} and g_{r_id} are modeled as N-Rayleigh fading channels. According to (5), (6), and (8), the PDFs of the SNRs are formulated as follows:

$$f_{\overline{\gamma}_{sr_i}}(x) \approx \frac{a_{sr_i}^m}{n\Gamma(m)} \sum_{k=1}^{\infty} \frac{(-a_{sr_i}^m)^k}{k!} x^{c-1+\frac{k}{n}}, \tag{17}$$

$$f_{\gamma_{r_id}}(x) \approx \frac{a_{r_id}^m}{n\Gamma(m)} \sum_{k=1}^{\infty} \frac{(-a_{r_id}^m)^k}{k!} x^{c-1+\frac{k}{n}}, \tag{18}$$

$$f_{\gamma_{r_i}}(x) = b_r \mathrm{e}^{-b_r x}, \tag{19}$$

where $a_{sr_i} = \frac{2m}{\Omega}(\frac{Q_{sr_i}N_r}{P_s\sigma_{sr_i}^2})^{\frac{1}{n}}$, $a_{r_id} = \frac{2m}{\Omega}(\frac{Q_{r_id}N_d}{P_r\sigma_{r_id}^2})^{\frac{1}{n}}$, and $b_r = \frac{N_r}{P_s\sigma_r^2}$. The CDF of $\overline{\gamma}_{sr_i}, \gamma_{r_id}$ and γ_{r_i} are given by

$$F_{\overline{\gamma}_{sr_i}}(x) \approx \frac{a_{sr_i}^m}{n\Gamma(m)} \sum_{k=1}^{\infty} \frac{(-a_{sr_i})^k x^{c+\frac{k}{n}}}{k!\left(c+\frac{k}{n}\right)}, \tag{20}$$

$$F_{\gamma_{r_id}}(x) \approx \frac{a_{r_id}^m}{n\Gamma(m)} \sum_{k=1}^{\infty} \frac{(-a_{r_id})^k x^{c+\frac{k}{n}}}{k!\left(c+\frac{k}{n}\right)}, \tag{21}$$

$$F_{\gamma_{r_i}}(x) = 1 - \mathrm{e}^{-b_{r_i}x}. \tag{22}$$

According to (7), (19), and (20), the CDF of γ_{sr_i} can be written as

$$\begin{aligned} F_{\gamma_{sr_i}}(x) =& \Pr\left[\frac{\overline{\gamma}_{sr_i}}{1+\gamma_{r_i}} < x\right] \\ =& \int_0^{\infty} F_{\overline{\gamma}_{sr_i}}[(y+1)x] f_{\gamma_{r_i}}(y)\mathrm{d}y \\ =& \frac{a_{sr_i}^m \mathrm{e}^{b_r}}{n\Gamma(m)} \sum_{k=1}^{\infty} \frac{(-a_{sr_i})^k x^{c+\frac{k}{n}}}{k!\left(c+\frac{k}{n}\right) b_r^{c+\frac{k}{n}}} \Gamma\left(1+c+\frac{k}{n}, b_r\right), \end{aligned} \tag{23}$$

where the expression is obtained from the integral equation $\int_u^{\infty} x^m \mathrm{e}^{-\beta x^n}\mathrm{d}x = \frac{\Gamma(v,\beta u^n)}{n\beta^v}, v = \frac{m+1}{n}$ in [38, Eq. (3.381-9)].

3 Relay selection and outage probability

The choice of relay selection strategy significantly influences the performance of full-duplex multi-relay communication systems. This work systematically investigates four representative strategies: max signal-to-interference-plus-noise ratio (MS), min loop-interference (ML), partial signal-to-interference-plus-noise ratio (PS), and the hybrid relay (HR) strategy. These approaches are distinguished by their selection criteria: the MS strategy maximizes the end-to-end signal-to-interference-plus-noise ratio (SINR); the ML strategy seeks to minimize loop interference; the PS strategy optimizes the SINR of a partial link, typically the first hop; and the HR strategy adaptively switches between FD and HD operation based on instantaneous link conditions. Consequently, these strategies exhibit significant trade-offs in terms of reliability, computational complexity, and adaptability to diverse deployment scenarios. To provide a comprehensive and intuitive comparison, Table 1 summarizes the key characteristics of these four strategies with respect to algorithmic complexity, signaling requirements, reliability, and their suitability for typical application environments. In addition, Figure 3 presents a unified horizontal flowchart that

Table 1 Comparison of relay selection strategies.

Strategy	Algorithmic complexity	Signaling overhead	Reliability	Applicability (typical scenarios)
MS	$\mathcal{O}(N)$	High	Medium-high	Urban static, channel-stable, moderate SI
ML	$\mathcal{O}(N)$	Medium-low	Medium-low	SI-dominated, sparse nodes, low mobility
PS	$\mathcal{O}(N)$	Low	Low	Static, low-interference, short-range, simple topology
HR	$\mathcal{O}(N)$	High	High	Dense, strong-interference, dynamic or high-mobility 6G

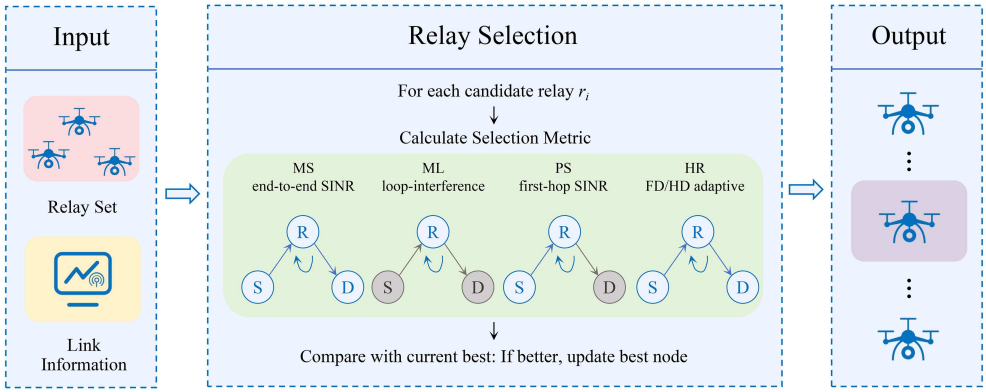

Figure 3 (Color online) General flowchart of relay selection. All strategies share the same process except for the selection metric.

visualizes the common relay-selection loop and highlights, within the decision block, the distinct selection metric employed by each strategy. This diagram complements Table 1 by clarifying where the four strategies diverge while sharing the same procedural framework.

In the remainder of this section, we investigate the differences in the reliability performance of the communication system under four relay selection strategies in the BMUM and MMUM scenarios, with outage probability as the reliability metric. For a given relay selection strategy, when the forwarding relay r_i is selected in a full-duplex multi-relay wireless communication system, the outage probability of the system can be expressed as follows:

$$\begin{aligned} P_{\Theta}^{\mathrm{DF}} &= \Pr\left(\min\left\{\gamma_{sr_{i_\Theta}}, \gamma_{r_{i_\Theta}d}\right\} < \gamma_{th}\right) \\ &= 1 - \Pr\left(\gamma_{sr_{i_\Theta}} > \gamma_{th}\right)\Pr\left(\gamma_{r_{i_\Theta}d} > \gamma_{th}\right), \end{aligned} \tag{24}$$

where r_{i_Θ} denotes the relay selected by the relay selection strategy Θ, and γ_{th} denotes the signal-to-noise ratio threshold.

The MS, ML, and PS strategies are exclusively operated in the FD mode; therefore, their outage probabilities can be directly computed using (24). In contrast, the HR strategy employs an adaptive mechanism to switch between FD and HD modes according to the instantaneous channel and interference conditions. Consequently, its outage analysis requires a dedicated methodology, which is detailed in the subsequent subsections.

3.1 Max signal-to-interference-plus-noise ratio strategy

The MS selection strategy uses maximizing the SNR as the basis for selecting a relay, and the relay node selected by this strategy can provide the maximum channel capacity for the system. The detail of this selection strategy is

$$i_{MS} = \arg\max_i \left\{\min\left\{\gamma_{sr_i}, \gamma_{r_i d}\right\}\right\}. \tag{25}$$

From the expression of the outage probability (24), it can be seen that when the SINR provided by the selected relay is less than the threshold γ_{th}, all the N relays in this communication system will fail to communicate normally. Based on the above analysis, we can derive the expression for the outage

probability under the MS selection strategy as

$$\begin{aligned} P_{\mathrm{MS}}^{\mathrm{DF}} &= \prod_{i=1}^{N} \left(\Pr\left(\min\left\{\gamma_{sr_i}, \gamma_{r_i d}\right\} < \gamma_{th}\right)\right) \\ &= \prod_{i=1}^{N} \left(1 - \Pr\left(\gamma_{sr_i} > \gamma_{th}\right) \Pr\left(\gamma_{r_i d} > \gamma_{th}\right)\right). \end{aligned} \tag{26}$$

• BMUM scenario

According to (14), (16) and (26), the outage probability based on the MS strategy in the BMUM scenario is

$$P_{\mathrm{MS}}^{\mathrm{DF}} = \prod_{i=1}^{N} \left[1 - \frac{b_r \mathrm{e}^{-b_{sr_i} x}}{b_r + b_{sr_i} x} \left(1 - \frac{a_{r_i d}^m}{n\Gamma(m)} \sum_{k=1}^{\infty} \frac{(-a_{r_i d})^k x^{c+\frac{k}{n}}}{k!\left(c+\frac{k}{n}\right)}\right)\right]. \tag{27}$$

• MMUM scenario

From expressions (21), (23) and (26), we can obtain the outage probability as

$$P_{\mathrm{MS}}^{\mathrm{DF}} = \prod_{i=1}^{N} \left[1 - \left(1 - \frac{a_{sr_i} \mathrm{e}^{b_r}}{n\Gamma(m)} \sum_{k=1}^{\infty} \frac{(-a_{sr_i})^k x^{c+\frac{k}{n}}}{k!\left(c+\frac{k}{n}\right) b_r^{c+\frac{k}{n}}} \Gamma\left(1+c+\frac{k}{n}, b_r\right)\right) \times \left(1 - \frac{a_{r_i d}^m}{n\Gamma(m)} \sum_{k=1}^{\infty} \frac{(-a_{r_i d})^k x^{c+\frac{k}{n}}}{k!\left(c+\frac{k}{n}\right)}\right)\right]. \tag{28}$$

3.2 Min loop-interference strategy

The ML selection strategy considers only the link r_i-r_i, and bases relay selection on the minimization of loop interference. As a result, the ML strategy will select a forwarding relay that satisfies the following equation:

$$i_{\mathrm{ML}} = \arg\min_{i} \left\{\gamma_{r_i}\right\}. \tag{29}$$

Therefore, according to expression (30), the SNR of the selected relay on the link r_i-r_i varies as

$$\begin{aligned} F_{\gamma_{r_{i_{\mathrm{ML}}}}}(x) &= 1 - \left[\Pr\left(\gamma_{r_{i_{\mathrm{ML}}}} < x\right)\right] \\ &= 1 - \mathrm{e}^{-N b_r x}. \end{aligned} \tag{30}$$

• BMUM scenario

Based on the expressions (7), (13) and (30), the CDF of $\gamma_{sr_{i_{\mathrm{ML}}}}$ can be written as

$$\begin{aligned} F_{\gamma_{sr_{i_{\mathrm{ML}}}}}(x) &= \int_0^{\infty} F_{\overline{\gamma}_{sr_i}}[(y+1)x] f_{\gamma_{r_{i_{\mathrm{ML}}}}}(y)\mathrm{d}y \\ &= 1 - \frac{N\mathrm{e}^{-b_{sr_{i_{\mathrm{ML}}}} x}}{N + x b_{sr_{i_{\mathrm{ML}}}}/b_r}. \end{aligned} \tag{31}$$

Therefore, the outage probability under the ML relay selection strategy is obtained as

$$\begin{aligned} P_{\mathrm{ML}}^{\mathrm{DF}} &= \Pr\left(\min\left\{\gamma_{sr_{i_{\mathrm{ML}}}}, \gamma_{r_{i_{\mathrm{ML}}}} d\right\} < \gamma_{th}\right) \\ &= 1 - \frac{N\mathrm{e}^{-b_{sr_{i_{\mathrm{ML}}}} \gamma_{th}}}{N + \gamma_{th} b_{sr_{i_{\mathrm{ML}}}}/b_r} \left(1 - \frac{a_{r_{i_{\mathrm{ML}}} d}^m}{n\Gamma(m)} \sum_{k=1}^{\infty} \frac{(-a_{r_{i_{\mathrm{ML}}} d})^k x^{c+\frac{k}{n}}}{k!\left(c+\frac{k}{n}\right)}\right). \end{aligned} \tag{32}$$

It is clear from the preceding expressions (32) that the selected relay's channel parameters are required to calculate the outage probability under the ML relay selection strategy; however, the selected relay cannot be determined without instantaneous channel data, and the channel parameters vary for each relay. As a result, two approximate expressions for the probability of an outage are provided.

$$P_{\mathrm{ML}_1}^{\mathrm{DF}} \approx \prod_{i=1}^{N} \left[1 - \frac{N\mathrm{e}^{-b_{sr_i} \gamma_{th}}}{N + \gamma_{th} b_{sr_i}/b_r} \times \left(1 - \frac{a_{r_i d}^m}{n\Gamma(m)} \sum_{k=1}^{\infty} \frac{(-a_{r_i d})^k x^{c+\frac{k}{n}}}{k!\left(c+\frac{k}{n}\right)}\right)\right]^{\frac{1}{N}}, \tag{33}$$

$$P_{\mathrm{ML}_2}^{\mathrm{DF}} \approx \sum_{i=1}^{N} \left[\frac{1}{N} - \frac{\mathrm{e}^{-b_{sr_i} \gamma_{th}}}{N + \gamma_{th} b_{sr_i}/b_r} \times \left(1 - \frac{a_{r_i d}^m}{n\Gamma(m)} \sum_{k=1}^{\infty} \frac{(-a_{r_i d})^k x^{c+\frac{k}{n}}}{k!\left(c+\frac{k}{n}\right)}\right)\right]. \tag{34}$$

• MMUM scenario

The CDF of γ_{sr_i} can be obtained by (7), (20) and (30) driven as

$$\begin{aligned} F_{\gamma_{sr_{i_{\mathrm{ML}}}}}(x) =& \int_0^{\infty} F_{\overline{\gamma}_{sr_{i_{\mathrm{ML}}}}}[(y+1)x] f_{\gamma_{r_{i_{\mathrm{ML}}}}}(y)\mathrm{d}y \\ =& \frac{a_{sr_{i_{\mathrm{ML}}}}\mathrm{e}^{Nb_r}}{n\Gamma(m)} \sum_{k=1}^{\infty} \frac{(-a_{sr_{i_{\mathrm{ML}}}})^k x^{c+\frac{k}{n}}}{k!\left(c+\frac{k}{n}\right)(Nb_r)^{c+\frac{k}{n}}} \Gamma\left(1+c+\frac{k}{n}, Nb_r\right). \end{aligned} \tag{35}$$

The outage probability under the ML relay selection strategy in the MMUM scenario can be driven as

$$\begin{aligned} P_{\mathrm{ML}}^{\mathrm{DF}} =& 1 - \left[1 - \frac{a_{sr_{i_{\mathrm{ML}}}}\mathrm{e}^{Nb_r}}{n\Gamma(m)} \sum_{k=1}^{\infty} \frac{(-a_{sr_{i_{\mathrm{ML}}}})^k x^{c+\frac{k}{n}}}{k!\left(c+\frac{k}{n}\right)(Nb_r)^{c+\frac{k}{n}}} \right. \\ & \left. \times \Gamma\left(1+c+\frac{k}{n}, Nb_r\right)\right] \left(1 - \frac{a_{r_{i_{\mathrm{ML}}}d}^m}{n\Gamma(m)} \sum_{k=1}^{\infty} \frac{(-a_{r_{i_{\mathrm{ML}}}d})^k x^{c+\frac{k}{n}}}{k!\left(c+\frac{k}{n}\right)}\right). \end{aligned} \tag{36}$$

Similarly, when the source node and destination node of the communication system are distant and the relay nodes are relatively clustered with each other, two approximate expressions for the outage probability can be obtained as

$$P_{\mathrm{ML}_1}^{\mathrm{DF}} \approx \prod_{k=1}^{N} \left\{ 1 - \left[1 - \tfrac{a_{sr_i}\mathrm{e}^{Nb_r}}{n\Gamma(m)} \sum_{k=1}^{\infty} \tfrac{(-a_{sr_i})^k}{k!\left(c+\frac{k}{n}\right)} \tfrac{x}{Nb_r}^{c+\frac{k}{n}} \Gamma\left(1+c+\tfrac{k}{n}, Nb_r\right)\right] \left(1 - \tfrac{a_{r_i d}^m}{n\Gamma(m)} \sum_{k=1}^{\infty} \tfrac{(-a_{r_i d})^k x^{c+\frac{k}{n}}}{k!\left(c+\frac{k}{n}\right)}\right) \right\}^{\frac{1}{N}}, \tag{37}$$

$$P_{\mathrm{ML}_2}^{\mathrm{DF}} \approx \sum_{k=1}^{N} \left\{ \tfrac{1}{N} - \tfrac{1}{N} \left[1 - \tfrac{a_{sr_i}\mathrm{e}^{Nb_r}}{n\Gamma(m)} \sum_{k=1}^{\infty} \tfrac{(-a_{sr_i})^k}{k!\left(c+\frac{k}{n}\right)} \tfrac{x}{Nb_r}^{c+\frac{k}{n}} \Gamma\left(1+c+\tfrac{k}{n}, Nb_r\right)\right] \left(1 - \tfrac{a_{r_i d}^m}{n\Gamma(m)} \sum_{k=1}^{\infty} \tfrac{(-a_{r_i d})^k x^{c+\frac{k}{n}}}{k!\left(c+\frac{k}{n}\right)}\right) \right\}. \tag{38}$$

3.3 Partial signal-to-interference-plus-noise ratio strategy

The main objective of the PS selection strategy is to provide the optimal first-hop SINR for the system, and compared with the ML selection strategy, link s-r_i is added as a consideration. Therefore, the selected relay satisfies the following condition:

$$i_{\mathrm{PS}} = \arg\max_i \{\gamma_{sr_i}\}. \tag{39}$$

According to previous analysis, the CDF of the first-hop SINR of the selected relay can be derived as

$$F_{\gamma_{sr_{i_{\mathrm{PS}}}}}(x) = \prod_{i=1}^{N} \Pr[\gamma_{sr_i} < x]. \tag{40}$$

• BMUM scenario

From the expressions (40) and (24), the outage probability of the communication system with the PS relay selection strategy in the BMUM scenario is

$$P_{\mathrm{PS}}^{\mathrm{DF}} = 1 - \left[1 - \prod_{i=1}^{N} \left(1 - \frac{b_r \mathrm{e}^{-b_{sr_i}\gamma_{th}}}{b_{sr_i}\gamma_{th} + b_r}\right)\right] \left(1 - \frac{a_{r_{i_{\mathrm{PS}}}d}^m}{n\Gamma(m)} \sum_{k=1}^{\infty} \frac{(-a_{r_{i_{\mathrm{PS}}}d})^k x^{c+\frac{k}{n}}}{k!\left(c+\frac{k}{n}\right)}\right). \tag{41}$$

Similar to the ML relay selection strategy, it is still not possible to determine the selected relay in the absence of instantaneous channel data; therefore, approximate expressions for the outage probability under the two PS selection strategies are given as

$$P_{\mathrm{PS}_1}^{\mathrm{DF}} \approx \prod_{k=1}^{N} \left\{ 1 - \left[1 - \textstyle\prod_{i=1}^{N} \left(1 - \tfrac{b_r \mathrm{e}^{-b_{sr_i}\gamma_{th}}}{b_{sr_i}\gamma_{th}+b_r}\right)\right] \left(1 - \tfrac{a_{r_i d}^m}{n\Gamma(m)} \textstyle\sum_{k=1}^{\infty} \tfrac{(-a_{r_i d})^k x^{c+\frac{k}{n}}}{k!\left(c+\frac{k}{n}\right)}\right) \right\}^{\frac{1}{N}}, \tag{42}$$

$$P_{\mathrm{PS}_2}^{\mathrm{DF}} \approx \sum_{k=1}^{N} \left\{ \tfrac{1}{N} - \tfrac{1}{N} \left[1 - \textstyle\prod_{i=1}^{N} \left(1 - \tfrac{b_r \mathrm{e}^{-b_{sr_i}\gamma_{th}}}{b_{sr_i}\gamma_{th}+b_r}\right)\right] \left(1 - \tfrac{a_{r_i d}^m}{n\Gamma(m)} \textstyle\sum_{k=1}^{\infty} \tfrac{(-a_{r_i d})^k x^{c+\frac{k}{n}}}{k!\left(c+\frac{k}{n}\right)}\right) \right\}. \tag{43}$$

• MMUM scenario

The expression of the outage probability in the MMUM scenario can be written as

$$P_{\mathrm{PS}}^{\mathrm{DF}}=1-\left(1-\frac{a_{r_id}^m}{n\Gamma(m)}\sum_{k=1}^{\infty}\frac{(-a_{r_id})^k x^{c+\frac{k}{n}}}{k!\left(c+\frac{k}{n}\right)}\right)\left\{1-\prod_{k=1}^{N}\left[\frac{a_{sr_i}\mathrm{e}^{b_r}}{n\Gamma(m)}\sum_{k=1}^{\infty}\frac{(-a_{sr_i})^k x^{c+\frac{k}{n}}}{k!\left(c+\frac{k}{n}\right)b_r^{c+\frac{k}{n}}}\Gamma\left(1+c+\frac{k}{n},b_r\right)\right]\right\}. \tag{44}$$

Two approximate expressions for the outage probability are given by

$$P_{\mathrm{PS}_1}^{\mathrm{DF}}\approx\prod_{k=1}^{N}\left\{1-\left(1-\frac{a_{r_id}^m}{n\Gamma(m)}\sum_{k=1}^{\infty}\frac{(-a_{r_id})^k x^{c+\frac{k}{n}}}{k!\left(c+\frac{k}{n}\right)}\right)\left[1-\prod_{k=1}^{N}\left(\frac{a_{sr_i}\mathrm{e}^{b_r}}{n\Gamma(m)}\sum_{k=1}^{\infty}\frac{(-a_{sr_i})^k}{k!\left(c+\frac{k}{n}\right)}\left(\frac{x}{b_r}\right)^{c+\frac{k}{n}}\Gamma\left(1+c+\frac{k}{n},b_r\right)\right)\right]\right\}^{\frac{1}{N}}, \tag{45}$$

$$P_{\mathrm{PS}_2}^{\mathrm{DF}}\approx\sum_{k=1}^{N}\left\{\frac{1}{N}-\frac{1}{N}\left(1-\frac{a_{r_id}^m}{n\Gamma(m)}\sum_{k=1}^{\infty}\frac{(-a_{r_id})^k x^{c+\frac{k}{n}}}{k!\left(c+\frac{k}{n}\right)}\right)\left\{1-\prod_{k=1}^{N}\left[\frac{a_{sr_i}\mathrm{e}^{b_r}}{n\Gamma(m)}\sum_{k=1}^{\infty}\frac{(-a_{sr_i})^k}{k!\left(c+\frac{k}{n}\right)}\left(\frac{x}{b_r}\right)^{c+\frac{k}{n}}\Gamma\left(1+c+\frac{k}{n},b_r\right)\right]\right\}\right\}. \tag{46}$$

3.4 Hybrid relay strategy

The HR relay selection strategy can switch between full-duplex and half-duplex communication methods to obtain the maximum channel capacity based on the instantaneous channel state information. This strategy can effectively reduce the negative effects of loop interference caused by full duplex communication mode. Therefore, the selected relay satisfies the following expression:

$$i_{\mathrm{HR}}=\arg\max_{i}\left\{\max\left\{C_i^{\mathrm{FD}},C_i^{\mathrm{HD}}\right\}\right\}, \tag{47}$$

where the channel capacity with half-duplex communication mode can be expressed as

$$C_i^{\mathrm{HD}}=\frac{1}{2}\log_2\left(1+\min\left\{\overline{\gamma}_{sr_i},\gamma_{r_id}\right\}\right). \tag{48}$$

According to the above, the outage probability of the communication system under the HR relay selection strategy can be written as

$$\begin{aligned}P_{\mathrm{HR}}^{\mathrm{DF}}&=\prod_{i=1}^{N}\Pr\left(\min(\overline{\gamma}_{sr_i},\gamma_{r_id})\leqslant x^2-1,\min\left(\gamma_{sr_i},\gamma_{r_id}\right)\leqslant x-1\right)\\&=\prod_{i=1}^{N}\left(\underbrace{F_{\mathrm{HR}_1}^{i}\left(1+\gamma_{th}\right)}_{\gamma_{r_i}<x}+\underbrace{F_{\mathrm{HR}_2}^{i}\left(1+\gamma_{th}\right)}_{\gamma_{r_i}\geqslant x}\right),\end{aligned} \tag{49}$$

where $P_{\mathrm{HR}}^{\mathrm{DF}}$ is divided into two components, denoted as $F_{\mathrm{HR}_1}^{i}$ and $F_{\mathrm{HR}_2}^{i}$, according to different values of γ_{r_i}. For $F_{\mathrm{HR}_1}^{i}$, under the condition of $\gamma_{r_i}<x$, it can be deduced that $(\gamma_{r_i}+1)(x-1)<x^2-1$, then the expression of $F_{\mathrm{HR}_1}^{i}$ can be derived as

$$\begin{aligned}&F_{\mathrm{HR}_1}^{i}(x)\\&=\int_0^x\Pr\left(\min(\overline{\gamma}_{sr_i},\gamma_{r_id})\leqslant x^2-1,\min\left(\frac{\overline{\gamma}_{sr_i}}{1+\gamma_r},\gamma_{r_id}\right)\leqslant x-1\right)f_{\gamma_{r_i}}(y)\mathrm{d}y\\&=\int_0^x\left(F_{\overline{\gamma}_{sr_i}}[(x-1)(y+1)]+F_{\gamma_{r_id}}(x-1)\right)f_{\gamma_{r_i}}(y)\,\mathrm{d}y-\int_0^x F_{\overline{\gamma}_{sr_i}}[(x-1)(y+1)]F_{\gamma_{r_id}}(x-1)f_{\gamma_{r_i}}(y)\,\mathrm{d}y\\&=\left[1-F_{\gamma_{r_id}}(x-1)\right]\int_0^x F_{\overline{\gamma}_{sr_i}}[(x-1)(y+1)]f_{\gamma_{r_i}}(y)\mathrm{d}y+F_{\gamma_{r_id}}(x-1)F_{\gamma_{r_i}}(x).\end{aligned} \tag{50}$$

Similarly, considering $\gamma_{r_i} > x$, it is deduced that the expression for $F^i_{\mathrm{HR}_2}$ is

$$\begin{aligned} F^i_{\mathrm{HR}_2}(x) =& \int_x^\infty \Pr\left(\min(\overline{\gamma}_{sr_i},\gamma_{r_i d}) \leqslant x^2-1, \min\left(\frac{\overline{\gamma}_{sr_i}}{1+\gamma_r},\gamma_{r_i d}\right) \leqslant x-1\right) \times f_{\gamma_{r_i}}(y)\mathrm{d}y \\ =& \int_x^\infty F_{\overline{\gamma}_{sr_i}}\left[(x-1)(y+1)\right] F_{\gamma_{r_i d}}(x^2-1) f_{\gamma_{r_i}}(y)\,\mathrm{d}y \\ &+ \int_x^\infty \left\{1 - F_{\overline{\gamma}_{sr_i}}[(x-1)(y+1)]\right\} F_{\gamma_{r_i d}}(x-1) f_{\gamma_{r_i}}(y)\,\mathrm{d}y \\ &+ \int_x^\infty \left[1 - F_{\gamma_{r_i d}}(x^2-1)\right] F_{\overline{\gamma}_{sr_i}}(x^2-1) f_{\gamma_{r_i}}(y)\,\mathrm{d}y. \end{aligned} \tag{51}$$

• BMUM scenario

The analytical expressions for $F^i_{\mathrm{HR}1}$ and $F^i_{\mathrm{HR}_2}$ in the BMUM scenario are as follows:

$$\begin{aligned} & F^i_{\mathrm{HR}_1}(x) \\ =& (1-\mathrm{e}^{-b_{r_i}x}) - b_{r_i}\mathrm{e}^{-b_{sr_i}(x-1)} \frac{1-\mathrm{e}^{-(b_{r_i}+b_{sr_i}(x-1))x}}{b_{r_i}+b_{sr_i}(x-1)} \left[1 - \frac{a^m_{r_i d}}{n\Gamma(m)} \sum_{k=1}^\infty \frac{(-a_{r_i d})^k (x-1)^{c+\frac{k}{n}}}{k!\left(c+\frac{k}{n}\right)}\right] \\ &+ \left(1-\mathrm{e}^{-b_{r_i}x}\right) \frac{a^m_{r_i d}}{n\Gamma(m)} \sum_{k=1}^\infty \frac{(-a_{r_i d})^k (x-1)^{c+\frac{k}{n}}}{k!\left(c+\frac{k}{n}\right)}, \end{aligned} \tag{52}$$

$$\begin{aligned} & F^i_{\mathrm{HR}_2}(x) \\ =& \frac{a^m_{r_i d}}{n\Gamma(m)} \sum_{l=1}^\infty \frac{(-a_{r_i d})^l}{l!\left(c+\frac{l}{n}\right)} \left[(x^2-1)^{\,c+\frac{l}{n}} - (x-1)^{\,c+\frac{l}{n}}\right] \left[\mathrm{e}^{-b_{r_i}x} - b_{r_i}\mathrm{e}^{-b_{sr_i}(x-1)} \frac{\mathrm{e}^{-(b_{r_i}+b_{sr_i}(x-1))x}}{b_{r_i}+b_{sr_i}(x-1)}\right] \\ &+ \mathrm{e}^{-b_{r_i}x} \left[\frac{a^m_{r_i d}}{n\Gamma(m)} \sum_{l=1}^\infty \frac{(-a_{r_i d})^l}{l!\left(c+\frac{l}{n}\right)} (x-1)^{\,c+\frac{l}{n}} + \mathrm{e}^{b_{sr_i}(x^2-1)}\right]. \end{aligned} \tag{53}$$

• MMUM scenario

Similarly, the expressions of $F^i_{\mathrm{HR}_1}$ and $F^i_{\mathrm{HR}_2}$ in MMUM scenario can be obtained as

$$\begin{aligned} & F^i_{\mathrm{HR}_1}(x) \\ =& \frac{a^m_{sr_i}\mathrm{e}^{b_r}}{n\Gamma(m)} \sum_{k=1}^\infty \frac{(-a_{sr_i})^k (x-1)^{c+\frac{k}{n}} b_r}{k!\left(c+\frac{k}{n}\right)(1+c+\frac{k}{n})} \Gamma\left(1+c+\frac{k}{n}, b_r x\right)\Big|_{x+1}^1 \left[1 - \frac{a^m_{r_i d}}{n\Gamma(m)} \sum_{k=1}^\infty \frac{(-a_{r_i d})^k (x-1)^{c+\frac{k}{n}}}{k!\left(c+\frac{k}{n}\right)}\right] \\ &+ \mathrm{e}^{-b_{r_i}x} \left[1 - \frac{a^m_{r_i d}}{n\Gamma(m)} \sum_{k=1}^\infty \frac{(-a_{r_i d})^k x^{c+\frac{k}{n}}}{k!\left(c+\frac{k}{n}\right)}\right], \end{aligned} \tag{54}$$

$$\begin{aligned} & F^i_{\mathrm{HR}_2}(x) \\ =& \frac{a^m_{sr_i}\mathrm{e}^{b_r}}{n\Gamma(m)} \sum_{k=1}^\infty \frac{(-a_{sr_i})^k (x-1)^{c+\frac{k}{n}}}{k!\left(c+\frac{k}{n}\right) b_r^{c+\frac{k}{n}}} \Gamma\left[1+c+\frac{k}{n}, b_r(1+x)\right] \frac{a^m_{r_i d}}{n\Gamma(m)} \sum_{l=1}^\infty \frac{(-a_{r_i d})^l}{l!\left(c+\frac{l}{n}\right)} \\ &\times \left[(x^2-1)^{\,c+\frac{l}{n}} - (x-1)^{\,c+\frac{l}{n}}\right] + \left[\frac{a^m_{r_i d}}{n\Gamma(m)} \sum_{k=1}^\infty \frac{(-a_{r_i d})^k (x-1)^{c+\frac{k}{n}}}{k!(c+\frac{k}{n})} + \frac{a^m_{sr_i}}{n\Gamma(m)} \sum_{l=1}^\infty \frac{(-a_{sr_i})^l}{l!(c+\frac{l}{n})} (x^2-1)^{c+\frac{l}{n}}\right. \\ &\left. - \frac{a^m_{r_i d} a^m_{sr_i}}{n^2\Gamma(m)^2} \sum_{k=1}^\infty \sum_{j=1}^\infty \frac{(-a_{r_i d})^k (-a_{sr_i})^j}{k!j!(c+\frac{k}{n})(c+\frac{j}{n})} (x^2-1)^{2c+\frac{k+j}{n}}\right] \mathrm{e}^{-b_{r_i}x}. \end{aligned} \tag{55}$$

The analytical framework presented in this paper is established based on the N-Rayleigh fading channel model, which effectively characterizes complex multipath propagation, particularly when relay nodes are deployed in dense clusters. Our modeling further incorporates large-scale A2G fading and the specific path loss characteristics of mmWave propagation. For analytical tractability, we assume that channel

state information (CSI) and self-interference (SI) are perfectly estimated for all relevant links and nodes. However, it is important to note that these idealized assumptions may limit the direct applicability of the analytical results in practical low-altitude or dense urban deployments. In practical UAV-assisted networks, frequent NLOS conditions due to building obstructions, rapidly varying multipath fading, and urban shadowing may not be fully captured by the N-Rayleigh model or by large-scale path loss assumptions. Additionally, dense relay clustering can exacerbate co-channel interference and channel correlation, further impacting the performance of relay selection strategies.

Moreover, in practical systems, channel estimation and SI measurement are subject to inevitable errors arising from noise, pilot contamination, hardware impairments, and rapidly time-varying channels—particularly in highly dynamic or dense urban scenarios. Such estimation errors can degrade the accuracy of relay selection, lead to suboptimal decisions, and cause a significant performance gap between analytical predictions and real-world operation. These factors collectively highlight the potential discrepancy between theoretical analysis and practical deployment. Future research should address these limitations by incorporating more realistic mobility and shadowing models, explicitly accounting for imperfect CSI and SI estimation, and analyzing the robustness of relay selection algorithms under urban interference and channel estimation uncertainty.

4 Simulation results

The communication process is simulated in this section using the assumed communication system parameters, and the closed expressions for the BMUM and MMUM scenarios discussed and derived earlier in this paper are simulated and the accuracy of their derivation via Monte Carlo methods is verified. In this simulation, the number of relays is set to 5, the SNR threshold value γ_{th} is 1, the carrier frequency $f = 28$ GHz, the speed of light c $= 3 \times 10^8$ m/s, $\alpha_{\text{atm}} = 0.5$ dB/km, $\alpha_{\text{rain}} = 2.3$ dB/km, the variance of noise $N_r = N_d = -100$ dBm, and the variance $\sigma_r^2 = 5 \times 10^{-13}$, $\sigma_{sr_i}^2 = \sigma_{r_i d}^2 = 2$. The horizontal distance between s and d is 1500 m, and the relays r are located 200 m apart on the median between the source and destination nodes s and d. The two communication scenarios proposed in this chapter, BMUM and MMUM, are both in dense urban environments, so the environmental parameters for path loss are set to $\alpha = 12.08$, $\beta = 0.11, \eta_{\text{LoS}} = 1.6$ dB, and $\eta_{\text{NLoS}} = 23$ dB.

As depicted in Figure 4, the outage probability derived from various relay selection strategies varies with height h, where $P_s = P_r = 1$ dB. The figure displays data in two forms: solid lines and markers, representing Monte Carlo simulation data and analytical derivation data, respectively. The data in the figure indicates that the mathematical analysis for the MS and HR strategies aligns with the simulation results, thus validating the accuracy of the derivations. For the ML and PS strategies, at altitudes below 400 m, there are significant discrepancies between the mathematical approximations and the Monte Carlo simulation results. This clearly demonstrates that in low-altitude environments, the analytical models for predicting system performance are limited, and environmental variables substantially impact system performance. In the complex and variable low-altitude scenarios, factors such as terrain undulation and building obstructions can significantly alter the signal propagation characteristics, making it difficult for the analytical models based on ideal assumptions to accurately depict the actual situation. In the FD relay system, the MS strategy achieves the lowest outage probability due to its comprehensive consideration of channel factors. This implies that comprehensively considering various channel parameters in the design of communication systems can effectively enhance system reliability and stability. By intelligently selecting relays with favorable channel conditions, the risk of signal transmission interruption can be minimized, thus ensuring the stable transmission of data. The ML strategy, however, focuses solely on loop interference, resulting in the poorest communication reliability. This reflects that during the relay selection process, if only a single factor is considered while ignoring other important influencing elements, the overall performance of the system will be severely compromised. The communication system is a complex integrated entity, with each part being interconnected and mutually influencing. A one-sided strategy is difficult to adapt to diverse application scenarios. The PS strategy considers the SINR of the first hop. Although its outage probability is higher than that of the MS strategy, its reliability is improved compared with the ML strategy. This indicates that when optimizing the performance of communication systems, rationally choosing key parameters for consideration can improve the system performance to a certain extent. Even if the optimal effect cannot be achieved, it can enhance the system's anti-interference ability and data transmission stability under specific conditions. The

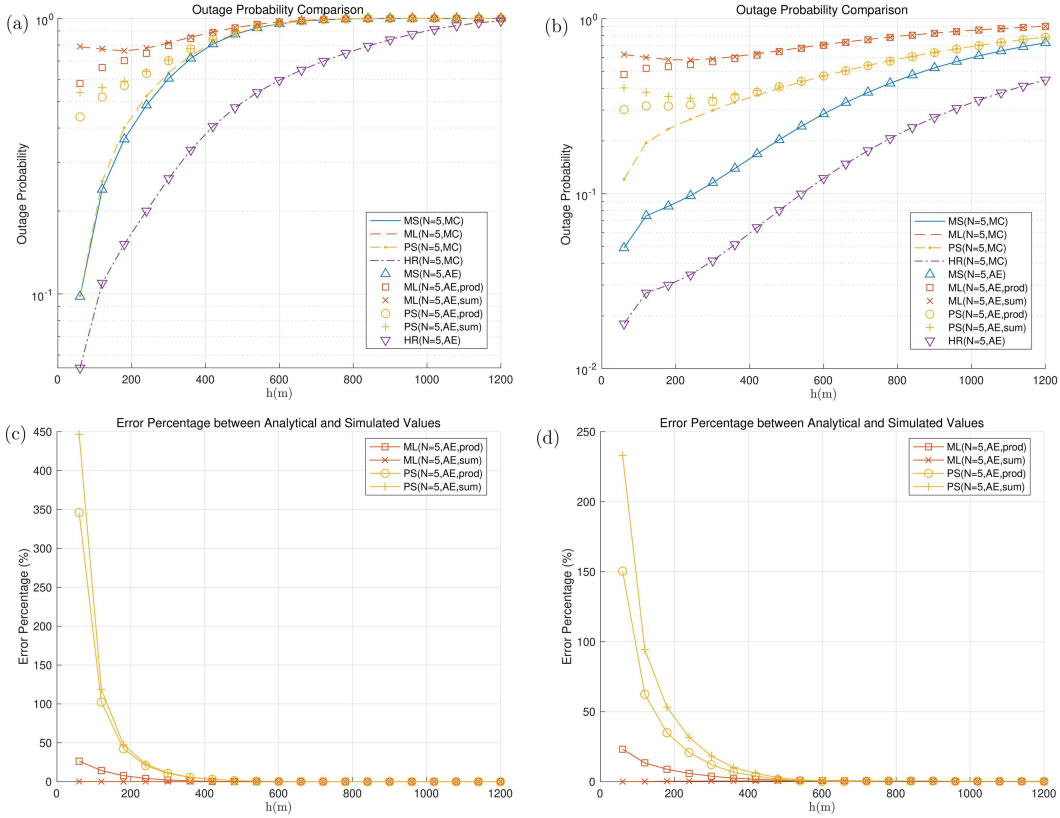

Figure 4 (Color online) Outage probability versus height with $n = 5, P_r = P_s = 1$. (a) BMUM; (b) MMUM; (c) BMUM; (d) MMUM.

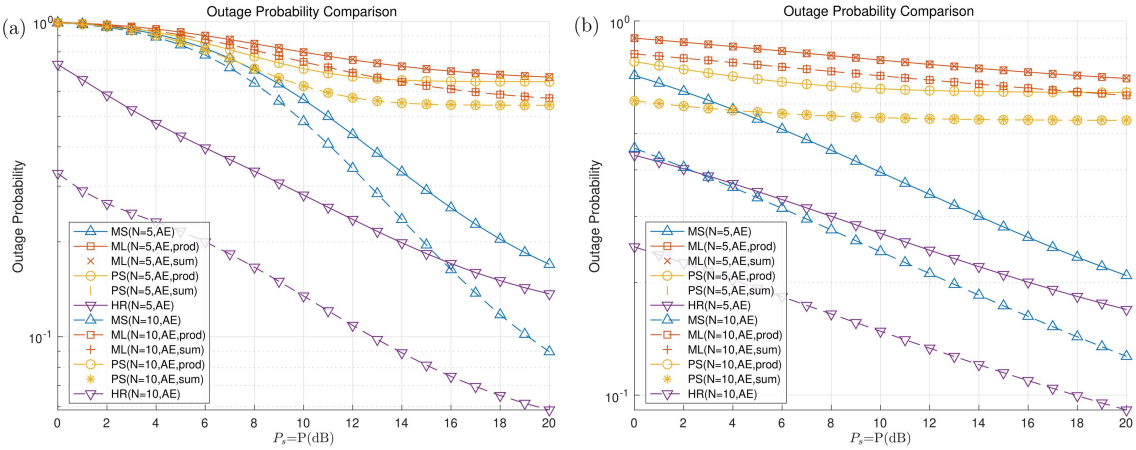

Figure 5 (Color online) Outage probability versus transmit power with $P_r = 1$ dB, $P_s = P$ (dB). (a) BMUM; (b) MMUM.

HR strategy operates in a hybrid FD and HD mode, enabling the relay to adjust its operating mode promptly based on channel state information, thereby effectively mitigating the adverse effects of loop interference on the communication system. This adaptive operating mode switching mechanism provides a new approach for constructing efficient and reliable communication systems. By dynamically adapting to channel changes, the HR strategy can flexibly balance transmission efficiency and anti-interference ability under different environmental conditions.

The analysis presented in Figures 5–7 is based on a fixed UAV altitude of $h = 500$ m. Figure 5 plots the outage probability as a function of the source-node transmit power P_s, while holding the relay-node power P_r constant. For a configuration with five relays ($N = 5$), the HR strategy significantly lowers the outage probability from 0.73 at $P_s = 0$ dB to 0.14 at $P_s = 20$ dB, representing an improvement of approximately

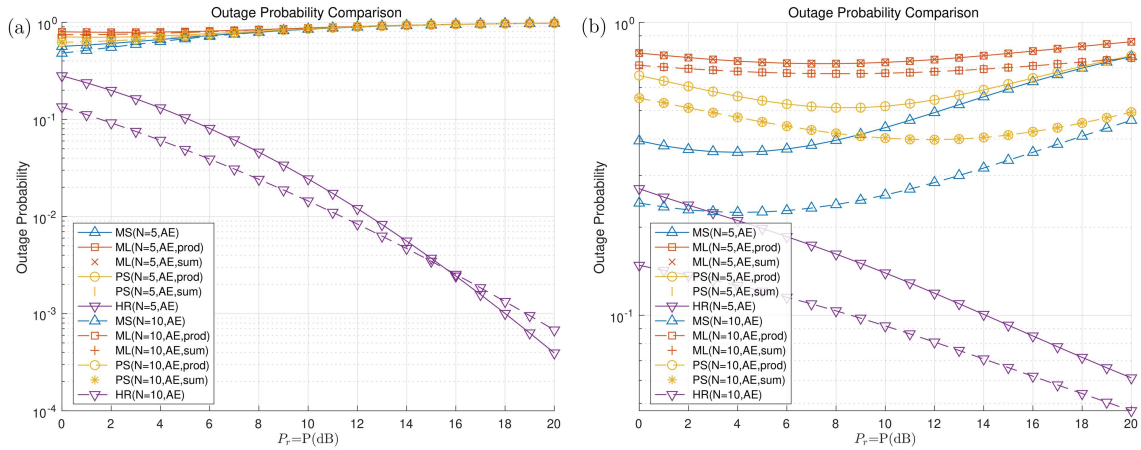

Figure 6 (Color online) Outage probability versus transmit power with $P_s = 10$ dB, $P_r = P$ (dB). (a) BMUM; (b) MMUM.

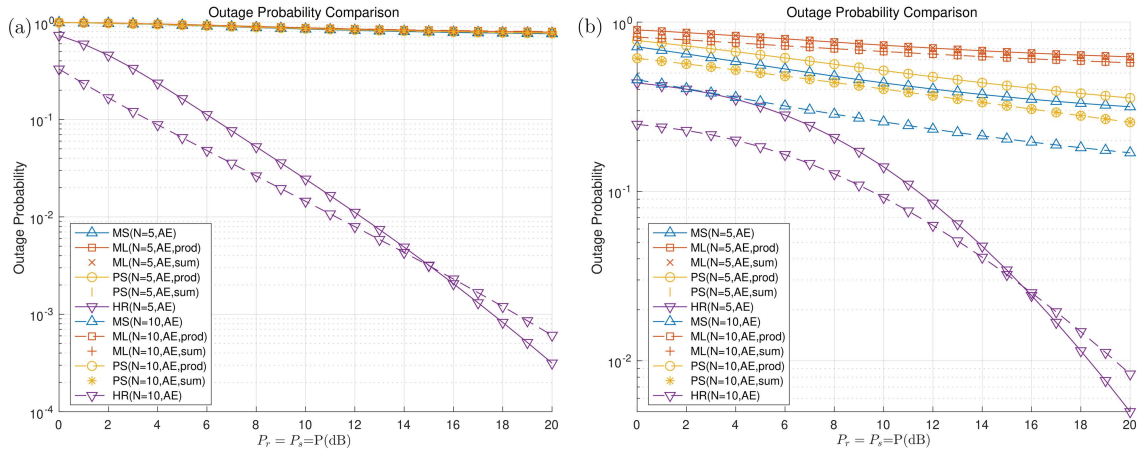

Figure 7 (Color online) Outage probability versus transmit power with $P_r = P_s = P$ (dB). (a) BMUM; (b) MMUM.

80%. In stark contrast, the MS benchmark exhibits markedly inferior performance across the entire power range, with its outage probability failing to drop below 0.99. Although the performance ratio of HR to MS improves from 0.26 to 0.80, parity is never achieved. Increasing the relay population to $N = 10$ further enhances the HR performance, shifting its curve downward; for instance, at $P_s = 20$ dB, the outage probability is reduced to 5.9×10^{-2}. Conversely, the ML and PS strategies show little sensitivity to the source power, as their outage probabilities remain above 0.64, which underscores the insufficiency of source-side power alone without explicit loop interference control.

Figure 6 investigates the impact of the relay-node transmit power P_r for a fixed source power of $P_s = 10$ dB. Two distinct operational regimes are evident. Below approximately 6 dB, all strategies benefit, as an increase in P_r strengthens the desired link more rapidly than it amplifies self-interference. Beyond this threshold, however, the performance of MS, ML, and PS degrades sharply, with their outage probabilities climbing to 0.98, 0.85, and 0.81, respectively, at $P_r = 20$ dB. The HR strategy, by contrast, circumvents this issue by detecting the onset of saturation and reverting to an HD mode. Consequently, for $N = 5$, its outage probability decreases monotonically from 0.28 to 3.9×10^{-4} over the same power span. The addition of five more relays yields a further 40%–50% reduction in outage probability, confirming the complementary nature of relay multiplicity and adaptive FD/HD switching.

Figure 7 explores the effect of jointly scaling both transmit powers, setting $P_s = P_r = P$, and contrasts the outcomes for $N = 5$ and $N = 10$. With the HR strategy, the outage probability improves by nearly an order of magnitude for every 10 dB increase in P. At $P = 20$ dB, it enters the ultra-reliable regime, reaching 3.2×10^{-4} for $N = 5$ and 6.1×10^{-5} for $N = 10$. The diminishing performance gap between the two HR cases at high power indicates that once self-interference is effectively suppressed, the marginal benefit of adding more relays lessens. In contrast, the other strategies remain ineffective, with outage probabilities consistently above 0.75, demonstrating that neither increased power nor additional relays

can overcome the lack of a robust interference mitigation mechanism.

In summary, the results from Figures 5–7 reveal a multi-faceted interplay between system parameters. While increasing source power is initially beneficial, its effectiveness is ultimately capped by interference from the relay's own transmit chain. Similarly, increasing relay power is only advantageous up to a critical threshold, beyond which naïve full-duplex systems suffer performance degradation. Furthermore, although a larger relay set is always helpful, its full potential is unlocked only by an interference-aware selection rule. By synergistically exploiting these three degrees of freedom—source power, relay power, and relay multiplicity—the HR strategy consistently achieves the minimum outage probability across the entire operational envelope.

5 Conclusion

Against the backdrop of the vigorous development of ISAC, this paper proposes two UAV-assisted full-duplex multi-relay mobile communication scenarios: the BMUM scenario, specifically designed for communication between the base station and mobile users (e.g., emergency response networks and urban base station offloading), and the MMUM scenario, aimed at communication between mobile ground users (e.g., disaster relief operations, temporary event coverage). These scenarios represent typical practical deployments of UAV-assisted relay networks in dense urban environments. In the proposed system model, the influences of UAV relays and complex urban propagation conditions are jointly considered by incorporating N-Rayleigh small-scale fading, UAV A2G path loss, mmWave path loss, and the impact of weather conditions on signal propagation. Under the BMUM and MMUM scenarios, we conduct an in-depth analysis of the communication reliability of the MS, PS, ML, and HR selection strategies. We derive the corresponding outage probability expressions through mathematical methods, and verify the accuracy of these derivations via simulations. Simulation results indicate that the ML strategy, focusing solely on the loop interference effect, yields the highest outage probability. In contrast, the PS strategy, which gives priority to the first hop, improves reliability compared to the ML strategy. The MS strategy, which comprehensively considers the channel information of both the first and second hops, achieves a lower system outage probability compared with the ML and PS strategies. The HR strategy effectively mitigates the severe impact of loop interference on the communication system, achieving the highest communication reliability. In practical engineering applications, particularly when the communication scenario demands extremely high real-time performance and allows for significant cost investment, the HR strategy is preferable as it significantly reduces outage probability and ensures communication continuity. For example, in real-time communication support for remote medical surgeries, stable and low-latency communication is of utmost importance. The HR strategy ensures stable data transmission during the surgical process, avoiding surgical risks caused by signal interruptions. If the communication scenario is under a limited budget and has relatively undemanding requirements for communication quality, the PS strategy can be given priority. For instance, in some temporary and simple data collection communication scenarios, the PS strategy can not only meet the basic communication needs but also control costs. The MS strategy demonstrates notable advantages in complex interference-rich urban environments, where a balance between the two-hop link performances is essential, such as in dense urban IoT deployments with multiple concurrent devices. It is important to note that the analytical framework in this work is developed under several idealized assumptions. In particular, the model assumes perfect channel state information and self-interference estimation, and does not account for estimation errors or hardware impairments. In practical low-altitude or dense urban deployments, frequent non-line-of-sight conditions, fast channel variations, and estimation errors may lead to deviations between the analytical predictions and actual system performance. Therefore, future research should focus on developing robust relay selection algorithms that account for imperfect channel knowledge, dynamic propagation environments, and real-world system constraints.

Acknowledgements This work was supported by National Natural Science Foundation of China (Grant No. 62371053).

References

1 Al-Fuqaha A, Guizani M, Mohammadi M, et al. Internet of Things: a survey on enabling technologies, protocols, and applications. IEEE Commun Surv Tutorials, 2015, 17: 2347–2376
2 Bao T, Wang H, Wang W J, et al. Secrecy outage performance analysis of UAV-assisted relay communication systems with multiple aerial and ground eavesdroppers. IEEE Trans Aerosp Electron Syst, 2022, 58: 2592–2600
3 Xiao Z, Zhu L, Liu Y, et al. A survey on millimeter-wave beamforming enabled UAV communications and networking. IEEE Commun Surv Tutorials, 2022, 24: 557–610

4 Al-Hourani A, Kandeepan S, Lardner S. Optimal LAP altitude for maximum coverage. IEEE Wireless Commun Lett, 2014, 3: 569–572
5 Li Q, Si P, Zhang Y, et al. UAV altitude, relay selection, and user association optimization for cooperative relay-transmission in UAV-IRS-based THz networks. IEEE Trans Green Commun Netw, 2024, 8: 815–826
6 Liu T, Cui M, Zhang G, et al. 3D trajectory and transmit power optimization for UAV-enabled multi-link relaying systems. IEEE Trans Green Commun Netw, 2021, 5: 392–405
7 Liang Y, Xiao L, Yang D, et al. Joint trajectory and resource optimization for UAV-aided two-way relay networks. IEEE Trans Veh Technol, 2022, 71: 639–652
8 Li B, Zhao S, Zhang R, et al. Joint transmit power and trajectory optimization for two-way multihop UAV relaying networks. IEEE Internet Things J, 2022, 9: 24417–24428
9 Ding R, Chen J, Wu W, et al. Packet routing in dynamic multi-hop UAV relay network: a multi-agent learning approach. IEEE Trans Veh Technol, 2022, 71: 10059–10072
10 Pan W, Lv N, Hou B, et al. Resource allocation and outage probability optimization method for multi-hop UAV relay network for servicing heterogeneous users. IEEE Trans Netw Sci Eng, 2024, 11: 2769–2781
11 Pan W, Lv N. Multi-UAV relay connectivity optimization for heterogeneous users based on load balancing and throughput maximization. IEEE Access, 2023, 11: 38944–38956
12 Sharma P K, Gupta D. Outage performance of multi-UAV relaying-based imperfect hardware hybrid satellite-terrestrial networks. IEEE Syst J, 2022, 16: 2311–2314
13 Ernest T Z H, Madhukumar A S, Sirigina R P, et al. Hybrid-duplex communications for multi-UAV networks: an outage probability analysis. IEEE Commun Lett, 2019, 23: 1831–1835
14 Yanmaz E. Dynamic relay selection and positioning for cooperative UAV networks. IEEE Netw Lett, 2021, 3: 114–118
15 Zhang G, Ou X, Cui M, et al. Cooperative UAV enabled relaying systems: joint trajectory and transmit power optimization. IEEE Trans Green Commun Netw, 2022, 6: 543–557
16 Yin D, Yang X, Yu H, et al. An air-to-ground relay communication planning method for UAVs swarm applications. IEEE Trans Intell Veh, 2023, 8: 2983–2997
17 Hu G, Cai Y. UAVs-assisted proactive eavesdropping in AF multi-relay system. IEEE Commun Lett, 2020, 24: 501–505
18 Lee D. Secrecy analysis of relay-user selection in AS-AF systems over Nakagami fading channels. IEEE Trans Veh Technol, 2021, 70: 2378–2388
19 Wang Z, Guo J, Chen Z, et al. Robust secure UAV relay-assisted cognitive communications with resource allocation and cooperative jamming. J Commun Netw, 2022, 24: 139–153
20 Kong L, Zou Y, Li B. Security and reliability tradeoff of UAV relays assisted cognitive transmissions with hardware impairments. IEEE Internet Things J, 2024, 11: 10336–10351
21 Wang S, Li L, Ruby R, et al. Secrecy-energy-efficiency maximization for UAV-enabled two-way relay systems. IEEE Trans Veh Technol, 2023, 72: 12900–12911
22 He Z, Ji Y, Wang K, et al. Energy minimization for UAV-enabled wireless power transfer and relay networks. IEEE Internet Things J, 2023, 10: 19141–19152
23 Ji X, Wang T. Energy minimization for fixed-wing UAV assisted full-duplex relaying with bank angle constraint. IEEE Wireless Commun Lett, 2023, 12: 1199–1203
24 Woo D H, Hwang H Y. A virtual full-duplex relaying scheme and adjustment algorithms for enhancing spectral efficiency in UAV-aided communication networks. IEEE Access, 2023, 11: 12698–12709
25 Sun G, Li J, Wang A, et al. Secure and energy-efficient UAV relay communications exploiting collaborative beamforming. IEEE Trans Commun, 2022, 70: 5401–5416
26 Huang X, Fu X. Fresh data collection for UAV-assisted IoT based on aerial collaborative relay. IEEE Sens J, 2023, 23: 8810–8825
27 Zhang R, Zhang Y, Tang R, et al. A joint UAV trajectory, user association, and beamforming design strategy for multi-UAV-assisted ISAC systems. IEEE Internet Things J, 2024, 11: 29360–29374
28 Li Y, Li X, Yang J, et al. Continuous UAV trajectory design with uncertain user location in ISAC networks. In: Proceedings of IEEE Wireless Communications and Networking Conference (WCNC), 2024. 1–6
29 Bayessa G A, Chai R, Liang C, et al. Joint UAV deployment and precoder optimization for multicasting and target sensing in UAV-assisted ISAC networks. IEEE Internet Things J, 2024, 11: 33392–33405
30 Liu Y, Liu X, Liu Z, et al. Secure rate maximization for ISAC-UAV assisted communication amidst multiple eavesdroppers. IEEE Trans Veh Technol, 2024, 73: 15843–15847
31 Duan X Y, Zhang X Q, Xia S Q, et al. Machine learning empowered UAV-based beamforming design in ISAC systems. Sci China Inf Sci, 2025, 68: 150307
32 Cui Y, Zhang Q, Feng Z, et al. Specific beamforming for multi-UAV networks: a dual identity-based ISAC approach. In: Proceedings of IEEE International Conference on Communications, 2023. 4979–4985
33 Wu Y W, Xu P, Lv Y, et al. Beamforming prediction based on the multireward DQN framework for UAV-RIS-assisted THz communication systems. Sci China Inf Sci, 2024, 67: 229303
34 Wang X, Chen H, Li S. Joint terminal-UAV association and power allocation for hybrid satellite-UAV relay network with rate splitting multiple access. IEEE Access, 2024, 12: 152668
35 Su Y, Liwang M, Chen Z, et al. Toward optimal deployment of UAV relays in UAV-assisted internet of vehicles. IEEE Trans Veh Technol, 2023, 72: 13392–13405
36 Wang B, Tao X F, Han S J, et al. Secure beamforming and deployment design for rate-splitting multiple access-based UAV communications. Sci China Inf Sci, 2025, 68: 112301
37 Li J, Niu Y, Wu H, et al. Joint optimization of relay selection and transmission scheduling for UAV-aided mmwave vehicular networks. IEEE Trans Veh Technol, 2023, 72: 6322–6334
38 Gradshteĭn I S, Zwillinger D. Table of Integrals, Series, and Products. 8th ed. Boston: Elsevier, 2015